International Journal of Integrated Academic Research
ISSN: 3139-5287 | Volume-1 Issue-2 | April-June 2026 | IAR12-005
doi: https://doi.org/10.5281/zenodo.22325761

GENERALIZED MAGNETOELECTRONIC CIRCUIT THEORY AND SPIN RELAXATION AT INTERFACES IN MAGNETIC MULTILAYERS

G.Divya , *IoT Research Associate, Dept of R&D,*
Newzen Infotech, Hyderabad

ABSTRACT: Spintronic devices that rely on spin transport at metal surfaces are thought to operate using spin pumping, spin-transfer torque, and extremely high magnetoresistance. In some of these devices, the relationship between spin and orbit is critical. To be more exact, spin-orbit coupling absorbs a small portion of the inbound spin current at the contact. By elaborating on the concept of spin-mixing conductance, we develop a full theory of magnetoelectronic circuits that describes the various ways that spin-flip scattering occurs. We present a simple equation that characterizes spin-mixing conductance in terms of the contributions that induce spin precession, spin torque, and spin relaxation, also known as spin memory loss. This is for the most prevalent type of exchange contact. Depending on the parameter that evaluates spin memory loss, spin-flip transfer and reflection are more or less likely to occur. Spin torque and spin memory loss are intricately linked. In the linear muffin-tin orbital technique, we use circuit theory to find and the Landauer-Büttiker method to find the spin-flip scattering rates for the interfaces N|N, F|N, and F|F.

Keywords: *Magnetoelectronic Circuit Theory, Spin Relaxation, Magnetic Multilayers, Spin Transport, Spin Accumulation, Spin-Dependent Transport, Interface Effects, Spin Diffusion, Magnetoresistance, Spintronics*

1. INTRODUCTION

Spin-orbit coupling (SOC) is the most important factor in spin-transport phenomena like giant magnetoresistance (GMR) [1,2], spin injection and accumulation [3,4], spin-transfer torque [5,6], spin pumping [7,8], spin Hall magnetoresistance (SMR) [10], and the spin Seebeck effect (SSE) [11-13]. Spin-mixing conductance developed as a substantial assist in magnetoelectronic circuit theory [14, 15] to promote spin motion on magnetic surfaces.

Nonetheless, when evaluating the spin-mixing conductance in its original form, substantial aspects remain inexplicable. These include spin-flip processes [16-22], lattice coupling [23, 24], and other magnon-related phenomena [25-27]. Examining spin pumping via the lens of spin-flip processes [28] or magnetoelectronic circuit theory through the lens of spin-flip scattering [29] is one method for improving understanding of spin-mixing conductance. In terms of interfacial spin relaxation, also known as spin memory loss or spin loss, the mechanics underpinning spin pumping and spin-transfer torque remain poorly understood, and such generalizations are insufficient. Recent advances in first-principles calculations of interfacial spin loss [29] indicate the need for the creation of an approach that encompasses

ISSN: 3139-5287 | Volume-1 Issue-2 | April-June 2026 | IAR12-005
doi: https://doi.org/10.5281/zenodo.22325761

fundamentally non-coherent processes. When there is insufficient theoretical support, experimental data on the correlation between spin-orbit contact and the efficacy of spin-orbit torque [18,30-32] are typically interpreted in terms of the spin memory loss parameter [1].

We investigate spin transport in multilayers using the most general form of magnetoelectronic circuit theory, with a focus on interfacial spin relaxation and spin-orbit torque. The generalized spin-mixing conductance is represented as a tensor. This explains spin-nonconserving phenomena like spin memory loss, spin precession, and spin dephasing. We employ the Landauer-Büttiker approach and the linear muffin-tin orbital (LMTO) method in the presence of spin-orbit interactions to determine the sections of the spin-mixing conductance that cause the loss of spin memory at the N|N, F|N, and F|F interfaces. In this paper, we show how to use generalized spin-mixing conductance to quantify spin-orbit torque in circumstances where exchange contacts predominate and lattice torque is not a relevant component. The results for generalized spin-mixing conductance show that fluctuations in scattering amplitudes contribute to both spin memory loss and torque, without establishing a conclusive correlation between the two. Section II describes how we included spin-flip scattering into a broader form of magnetoelectronic circuit theory. In Section III, we use magnetoelectronic circuit theory to compute the amount of spin loss in multilayers of (N1N2)N, (N1F2)N, or (F1F2)N coupled to ferromagnetic leads. Section IV calculates the spin-orbit force using magneto-electronic circuit theory. Section V delves into complicated computer difficulties, whereas Section VI delves into the technical details of the adiabatic-embedding technique. Section VII quantifies the spin-flip transmission and reflection rates, as well as the area-resistance products, for the N|N, F|N, and F|F surfaces, while Section VIII concludes the article.

2. GENERALIZED CIRCUIT THEORY

Formalism

The border conditions that define the linkages between pairs of nodes within a circuit are the foundation of magnetoelectronic circuit theory [14]. This section explains spin-orbit interaction, also known as nonuniform magnetization, which allows magnetic and nonmagnetic metals to interact without preserving spin. The boundary condition is: fa, where a = 1 and 2 represent the nodes, may form the boundary between nodes 1 and 2.

$$\hat{I}_2 = G_0 \sum_{nm} \{\hat{i}'_{mn}\hat{f}_1(\hat{i}'_{mn})^{\dagger} - [M_2\hat{f}_2 - \hat{r}_{mn}\hat{f}_2(\hat{r}_{mn})^{\dagger}]\}, \quad (1)$$

where $G_0 = e^2/h, \hat{r}_{mn}$ The number of electrons passing from channel n in node 1 to channel m in node 2 is shown by the amplitude of spin-dependent transmission (mn). Identifying the Hermitian counterpart is only possible in spin space. Determine the magnitude of spin-dependent reflection encountered by electrons when they travel from node 2's channel n to channel m. Equation (1) is easily adjusted to include the current I1 in node 1. The quantization of spin accumulation at a ferromagnetic node is thought to be inextricably tied to its magnetic strength. rmn and t rmn are two

International Journal of Integrated Academic Research
ISSN: 3139-5287 | Volume-1 Issue-2 | April-June 2026 | IAR12-005
doi: https://doi.org/10.5281/zenodo.22325761

matrices found commonly in spin space in an off-diagonal orientation. The distribution functions in the nodes, given by fa = L 0 f 0 a + L fs a, are commonly thought to be isotropic, suggesting that they are independent of k. Equation (1) can be simplified to the more generic Kirchhoff relations [29] in this case.

$$I_2^0 = G_2^{cc}\Delta f^0 + \mathbf{G}_2^{cs}\cdot\Delta\mathbf{f}^s - \mathbf{G}_2^m\cdot\mathbf{f}_2^s, \quad (2)$$

$$\mathbf{I}_2^s = \mathbf{G}_2^{sc}\Delta f^0 + \hat{\mathcal{G}}_2^{ss}\cdot\Delta\mathbf{f}^s - \hat{\mathcal{G}}_2^m\cdot\mathbf{f}_2^s, \quad (3)$$

The conductances in equations (2) and (3) are denoted by a subscript 2. This reveals that their conductances are significantly different from those shown in node 1. The subscript 2 will be removed from cases where this differentiation does not cause confusion. The distribution function is represented by the spin components and interfacial droplets of charge, written as fs = fs 1 fs 2. Conductances are related to the vector, scalar, and tensor values denoted by Gcs = Gsc Gt, Grss = Gcc 0 Grt, Grm = Grt + Grr, and Grm = Grt + Grr.

$$G^{cc} = 2G_0\sum_{mn}\mathcal{T}_{mn}^{vv}, \quad (4)$$

$$G_i^t = 4G_0\sum_{mn} i\varepsilon_{ijk}\mathcal{T}_{mn}^{jk}, \quad (5)$$

$$G_i^r = 4G_0\sum_{mn} i\varepsilon_{ijk}\mathcal{R}_{mn}^{jk}, \quad (6)$$

$$G_i^{sc} = 2G_0\sum_{mn}\left(\mathcal{T}_{mn}^{i0} + \mathcal{T}_{mn}^{0i} + i\varepsilon_{ijk}\mathcal{T}_{mn}^{jk}\right), \quad (7)$$

$$\mathcal{G}_{ij}^t = 2G_0\delta_{ij}^{kl}\sum_{mn}\left(\mathcal{T}_{mn}^{kl} + \mathcal{T}_{mn}^{lk} + i\varepsilon_{klp}\left[\mathcal{T}_{mn}^{0p} - \mathcal{T}_{mn}^{p0}\right]\right), \quad (8)$$

$$\mathcal{G}_{ij}^r = 2G_0\delta_{ij}^{kl}\sum_{mn}\left(\mathcal{R}_{mn}^{kl} + \mathcal{R}_{mn}^{lk} + i\varepsilon_{klp}\left[\mathcal{R}_{mn}^{0p} - \mathcal{R}_{mn}^{p0}\right]\right), \quad (9)$$

Cartesian coordinates are represented by the Latin numbers i through l, whereas conduction channels are represented by the letters m and n. The sum of Cartesian numbers that have been replicated above and below. As a result, kl i j equals i jkl ik jl. The following categories of dispersion matrix elements were developed using the aforementioned formulas:

$$\mathcal{R}_{mn}^{\mu\nu} = \mathrm{Tr}[(\hat{r}_{mn}\otimes\hat{r}_{mn}^*)\cdot(\hat{\sigma}^\mu\otimes\hat{\sigma}^\nu)]/4, \quad (10)$$

$$\mathcal{T}_{mn}^{\mu\nu} = \mathrm{Tr}[(\hat{t}_{mn}'\otimes\hat{t}_{mn}'^*)\cdot(\hat{\sigma}^\mu\otimes\hat{\sigma}^\nu)]/4, \quad (11)$$

As a result, Greek numerals can take on any value between zero and three. The trace relations for Pauli matrices were used to obtain Equations (2) and (3) for circuit theory: Tr(i T j) = 2i j, Tr(i j k) = 2iijk, and Tr(Apothekei j k l) = 2 (i jkl + iljk ik jl). According to the unitarity criteria, the following titles are required:

$$\sum_{mn}\hat{r}_{mn}\hat{r}_{mn}^\dagger + \hat{t}_{mn}'(\hat{t}_{mn}')^\dagger = M_2\hat{\sigma}^0, \quad (12)$$

$$\sum_{mn}\hat{r}_{mn}'(\hat{r}_{mn}')^\dagger + \hat{t}_{mn}(\hat{t}_{mn})^\dagger = M_1\hat{\sigma}^0, \quad (13)$$

$$\sum_{mn}\hat{r}_{mn}(\hat{r}_{mn})^\dagger + \hat{t}_{mn}(\hat{t}_{mn})^\dagger = M_2\hat{\sigma}^0, \quad (14)$$

$$\sum_{mn}\hat{r}_{mn}'(\hat{r}_{mn}')^\dagger + \hat{t}_{mn}'(\hat{t}_{mn}')^\dagger = M_1\hat{\sigma}^0, \quad (15)$$

This connects the conductances of the two nodes separated by the interface: Gcc 1 = Gcc 2, Gcs 1 + Gm 2, and Gcs 2 = Gcs 1 + Gm 1. To simplify comparisons between ab initio and actual results [35], the interface conductances in magnetoelectronic circuit theory must be renormalized. This can be accomplished by using the Sharvin resistance for unambiguous Ohmic connections [33, 34]. The conductances Gcc, Gcs, Gsc, Gm, Grss, and Gm can be renormalized to account for drift factors in the nodes. Equations (2) and (3)'s circuit theory can thus be applied to a broader range of situations. Using clear contacts, connect nodes 1 and 2 to the relevant pools, which contain spin-dependent distribution functions fL and fR. Following that, the currents passing through the nodes are denoted as I1 = 2G0M 1 (fL f1) and I2 = 2G0M 2 (f2 fR), with M 1(2) signifying the total number of spin-dependent

International Journal of Integrated Academic Research
ISSN: 3139-5287 | Volume-1 Issue-2 | April-June 2026 | IAR12-005
doi: https://doi.org/10.5281/zenodo.22325761

channels present in each node. As a result, there are practical alternatives to equations. (2) and (3) state that if f = (), f = () 1 plus I () 1 divided by (2G0M()1), and if f = (), f = () 2 minus I () 2 divided by (2G0M()2). Finally, it was established that the conductance Gm characterizes, among other spin-nonconserving events, spin dephasing, spin precession, and spin loss. Thus, it may be thought of as an extension of the tensor principle to systems where the spin-mixing constant can be changed by spin-flip scattering [14,36,37]. Regarding the specific instance studied in Reference [28], our model can be simplified to the proposed generalized tensor expression. Our perspective, on the other hand, is more comprehensive because it includes spin memory loss and spin precession. The conductances Gm and Gcs are examples of spin-charge conversion; this phenomena is also known as the spin galvanic effect. This phenomenon can be caused by processes that do not conserve spin. The tensor spin conductance is also denoted as Grss, whereas the inverse spin galvanic effect converts the charge imbalance into a spin current, which is denoted as Gsc.

Spin-conserving F|N interface

The theory of generalized circuits is currently in use on the connection F|N. If SO(3) rotates in spin space, Equations (2) and (3) should remain unchanged, unless a spin-conserving interface exists that behaves similarly to the theory of spin-conserving circuits [14,36,37]:

$$\mathbf{G}^{m} = 0, \tag{16}$$

$$\mathbf{G}^{cs} = \mathbf{G}^{sc} = G^{sc}\mathbf{m}, \tag{17}$$

$$\hat{\mathcal{G}}^{ss} = G^{cc}\,\mathbf{m}\otimes\mathbf{m}, \tag{18}$$

$$\hat{\mathcal{G}}^{m} = 2\mathcal{G}_{r}^{\uparrow\downarrow}(\hat{1}-\mathbf{m}\otimes\mathbf{m}) + 2\mathcal{G}_{i}^{\uparrow\downarrow}\mathbf{m}\times, \tag{19}$$

The symbols G r and G i denote the real and imaginary spin-mixing conductance components, respectively. The vector m m is defined by a projection onto the direction of magnetization. G0 mn (nm r mn mn t mn mn) = G.

General F|N interface

The F|N interface is frequently used.

The conductances of the vector and tensor components rise as the

$$G_{i}^{\alpha} = G_{i}^{\alpha(0)} + G_{i,k}^{\alpha(1)}m_{k} + G_{i,kl}^{\alpha(2)}m_{k}m_{l} + \cdots, \tag{20}$$

$$\mathcal{G}_{ij}^{\beta} = \mathcal{G}_{ij}^{\beta(0)} + \mathcal{G}_{ij,k}^{\beta(1)}m_{k} + \mathcal{G}_{ij,kl}^{\beta(2)}m_{k}m_{l} + \cdots, \tag{21}$$

The conductances of the vector and tensor components rise as the magnetic strength increases. This clarifies the current reaction setup.

When the system's nonmagnetic point group is studied, the tensors G(0) i, G(1) i,k, G(2) i,kl, G3(0) i j, G3(1) i j,k, G2(2) i j,kl, and others remain unchanged. The symbol "" indicates sc, cs, t, r, or m, whereas "2" represents ss, t, r, or m. Because of the axialsymmetry of the metric surfaces, understanding circuit theory is greatly aided in polycrystalline heterostructures. It is possible to enhance the vector conductances Gsc, Gsc, and Gm by two orders of magnitude by applying the constraints associated with the Cv geometry and designating the z line as the interface normal.

International Journal of Integrated Academic Research
ISSN: 3139-5287 | Volume-1 Issue-2 | April-June 2026 | IAR12-005
doi: https://doi.org/10.5281/zenodo.22325761

$$\vec{G}^{\alpha} = \begin{pmatrix} m_x x_1^{\alpha(1)} + m_y m_z x_1^{\alpha(2)} \\ m_y x_1^{\alpha(1)} - m_x m_z x_1^{\alpha(2)} \\ m_z x_2^{\alpha(1)} \end{pmatrix}, \quad (22)$$

Each of the coefficients x(1) 1, x(2) 1, and x(1) 2 is assumed to be at random. Components for the tensor conductances Grm and Gss are found for perpendicular and in-plane orientations, respectively.

$$\hat{\mathcal{G}}^{\beta} = \begin{pmatrix} x_1^{\beta(0)} & 0 & 0 \\ 0 & x_1^{\beta(0)} & 0 \\ 0 & 0 & x_2^{\beta(0)} \end{pmatrix} \quad (23)$$

$$+ \begin{pmatrix} 0 & -m_z x_1^{\beta(1)} & m_y x_2^{\beta(1)} \\ m_z x_1^{\beta(1)} & 0 & -m_x x_2^{\beta(1)} \\ -m_y x_3^{\beta(1)} & m_x x_3^{\beta(1)} & 0 \end{pmatrix} \quad (24)$$

$$+ \begin{pmatrix} m_x^2 x_1^{\beta(2)} + m_z^2 x_2^{\beta(2)} & m_x m_y x_1^{\beta(2)} & m_x m_z x_4^{\beta(2)} \\ m_x m_y x_1^{\beta(2)} & m_y^2 x_1^{\beta(2)} + m_z^2 x_2^{\beta(2)} & m_y m_z x_4^{\beta(2)} \\ m_x m_z x_5^{\beta(2)} & m_y m_z x_5^{\beta(2)} & m_z^2 x_3^{\beta(2)} \end{pmatrix}, \quad (25)$$

where $x_1^{\beta(0)}, x_2^{\beta(0)}, x_1^{\beta(1)}, x_2^{\beta(1)}, x_3^{\beta(1)}, x_1^{\beta(2)}, x_2^{\beta(2)}, x_3^{\beta(2)}, x_4^{\beta(2)}$, and $x_5^{\beta(2)}$ are arbitrary coefficients.

When the buildup of spin and magnetization is perpendicular to or parallel to the contact, the operation of spin-flip scattering is most visible. Equivalent results can be achieved by simplifying the tensor and vector conductances in Equations (2) and (3).

$$G^{cc} = G_0(T_{\uparrow\uparrow} + T_{\downarrow\downarrow} + T_{\uparrow\downarrow} + T_{\downarrow\uparrow}), \quad (26)$$

$$G^{sc} = G_0(T_{\uparrow\uparrow} - T_{\downarrow\downarrow} + T_{\uparrow\downarrow} - T_{\downarrow\uparrow}), \quad (27)$$

$$G^{t} = 2G_0(T_{\uparrow\downarrow} - T_{\downarrow\uparrow}),\ G^{r} = 2G_0(R_{\uparrow\downarrow} - R_{\downarrow\uparrow}), \quad (28)$$

$$\mathcal{G}^{t} = 2G_0(T_{\uparrow\downarrow} + T_{\downarrow\uparrow}),\ \mathcal{G}^{r} = 2G_0(R_{\uparrow\downarrow} + R_{\downarrow\uparrow}), \quad (29)$$

Extra parts are Gm = Gt + Gr, Gcs = Gsc Gt, and Gss = Gcc Gt. The values for magnetization in-plane and perpendicular orientations are fundamentally distinct in these formulations. The relevant index has been omitted to reduce extraneous data. The spin-resolved and size-independent transmittances and reflectances

$$T_{\sigma\sigma'} = \sum_{mn} t_{mn}^{\sigma\sigma'} \left(t_{mn}^{\sigma\sigma'}\right)^*, \quad (30)$$

$$R_{\sigma\sigma'} = \sum_{mn} r_{mn}^{\sigma\sigma'} \left(r_{mn}^{\sigma\sigma'}\right)^* \quad (31)$$

possess a quantization axis for spins that is parallel to the reference frame's magnetization. Equations (26-29) and (2) and (3) can be used to describe F|F surfaces that are symmetric along the x-axis by aligning the magnetizations of two ferromagnets. Axially symmetric N|N junction results from Reference [29] are generalized by including F|N and F|F interfaces into these formulations.

Relation to Valet-Fert theory

Spin relaxation in diffusive bulk regions is included in the Valet-Fert model [38]. However, its functioning is confined to interfaces, as it perceives them to be stable and transparent for spin, and therefore precludes the accumulation of transverse spin [2,16,39–42]. The Valet-Fert model solution is not universally applicable, even for N|N interfaces [29], due to the necessity of substituting interfaces with fictional bulk areas in circumstances when spin relaxation at interfaces is large [1, 2]. This section explains how diffusive bulk areas can be introduced into extended circuit theory. Whole devices displaying spin relaxation in the diffusive bulk regions and arbitrary spin-nonconserving scattering at the interfaces can be investigated using the modified Kirchhoff's principles [2,16,39–42]. For this purpose, nodes are positioned in proximity to the interfaces; the aggregate areas and interfaces are considered connections in and of themselves. The subsequent equations are applied by the Valet-Fert model to illustrate the

International Journal of Integrated Academic Research
ISSN: 3139-5287 | Volume-1 Issue-2 | April-June 2026 | IAR12-005
doi: https://doi.org/10.5281/zenodo.22325761

dispersion of charge and spin in a nonmagnetic metal:

$$\partial_x^2\left(Df_0^N\right)=0, \tag{32}$$

$$\frac{\partial^2}{\partial x^2}\left(D\mathbf{f}_s^N\right)=\frac{\mathbf{f}_s^N}{\tau_{sf}^N}, \tag{33}$$

analogous within a ferromagnet

$$\frac{\partial^2}{\partial x^2}\left(D_\uparrow f_\uparrow+D_\downarrow f_\downarrow\right)=0, \tag{34}$$

$$\frac{\partial^2}{\partial x^2}\left(D_\uparrow f_\uparrow-D_\downarrow f_\downarrow\right)=\frac{f_\uparrow-f_\downarrow}{\tau_{sf}^F}. \tag{35}$$

In this instance, the accumulation of spin is denoted by fF s = m(f↤ → f↤)/2. By employing the spin-diffusion lengths l N s f and l F s f, the diffusion coefficients D and Dς, and the fractional parts per million (1/2) N s f and ϱ F s f, it is possible to ascertain the duration of spin-flip relaxation. Let us now examine three critical components of a circuit. 1. The dispersed region N Equations (32) and (33) are more comprehensible upon converting the tensor conductances Gsc, Gsc, and Gm to scalars. Determining the solutions to equations (32) and (33) pertaining to a diffusive N layer is as follows:

$$G_N^{cc}=\frac{2D}{t_N}, \tag{36}$$

$$\mathcal{G}_N^{ss}=G_N^{cc}\frac{\delta_N}{\sinh\delta_N}, \tag{37}$$

$$\mathcal{G}_N^{m}=G_N^{cc}\,\delta_N\tanh\frac{\delta_N}{2}, \tag{38}$$

where t_N is the thickness of the N layer, and $\delta_N=t_N/l_{sf}^N$.

Diffusive F region

When equations (34) and (35) are solved in the case of a diffusive F layer with spin accumulation that is parallel to the magnetization, the conductance Gm disappears and the subsequent conductances appear.

$$G_F^{cc}=(D_\uparrow+D_\downarrow)/t_F, \tag{39}$$

$$\mathbf{G}_F^{sc}=\mathbf{G}_F^{cs}=\mathbf{m}(D_\uparrow-D_\downarrow)/t_F, \tag{40}$$

$$\mathcal{G}_F^{ss}=G_F^{*}\frac{\delta_F}{\sinh\delta_F}+\frac{\left(G_F^{sc}\right)^2}{G_F^{cc}}, \tag{41}$$

$$\mathcal{G}_F^{m}=G_F^{*}\,\delta_F\tanh\frac{\delta_F}{2}, \tag{42}$$

The effective conductance is denoted by G⋖ F = [(Gcc F) 2 → (Gsc F) 2]/Gcc F and σF = tF /l F s f. tF denotes the thickness of the F layer. It is noteworthy that these relationships demonstrate T←↔T↤↤ = T2 ←↤ within the μF 1 limit, as discussed in reference [43].

Diffusive F|N junction

To illustrate, consider the following scenario: a composite junction comprises diffusive layers F and N, which are visually isolated by a transparent surface. It is possible to illustrate the interface with spin-flip dispersion between the F and N layers using a hypothetical junction [2,16,39–42]. Effective conductance Gm = 0 when the boundary conditions are satisfied; the subsequent values are obtained by adding the outcomes from the F and N regions:

$$G^{cc}=\left(1/G_F^{cc}+1/G_N^{cc}\right)^{-1}, \tag{43}$$

$$\mathbf{G}^{cs}=\mathbf{G}^{sc}=\mathbf{G}_F^{sc}, \tag{44}$$

$$\hat{\mathcal{G}}^{ss}=\frac{\mathcal{G}_N^{ss}\mathcal{G}_F^{ss}}{\mathcal{G}_N^{ss}+\mathcal{G}_F^{ss}+\mathcal{G}_N^{m}+\mathcal{G}_F^{m}}\mathbf{m}\otimes\mathbf{m}, \tag{45}$$

$$\hat{\mathcal{G}}^{m}=\mathcal{G}_N^{ss}+\mathcal{G}_N^{m}-\frac{\mathcal{G}_N^{ss}\left(\mathcal{G}_N^{ss}+\mathcal{G}_F^{ss}\right)}{\mathcal{G}_N^{ss}+\mathcal{G}_F^{ss}+\mathcal{G}_N^{m}+\mathcal{G}_F^{m}}\mathbf{m}\otimes\mathbf{m}, \tag{46}$$

At a time when the conductances of the preceding components are required for the F and N layers. When spin-flip dispersion is extremely small, the well-known result [16] is obtained. N (1 → m → m) is

International Journal of Integrated Academic Research
ISSN: 3139-5287 | Volume-1 Issue-2 | April-June 2026 | IAR12-005
doi: https://doi.org/10.5281/zenodo.22325761

equivalent to G。m.

3. SPIN LOSS AT INTERFACES

The interfacial spin relaxation findings mostly come from measuring magnetoresistance in (N1N2)N, (N1F2)N, or (F1F2)N multilayers connected to ferromagnetic leads [1,2]. Here, N is the repetition number. In [1,2], the results were shown in terms of the effective spin memory loss parameter N or F. This was found by treating the interface as a fake bulk layer and fitting the data to the Valet-Fert model. In this part, we link the parameter N or F that was measured experimentally to the more general conductances shown in Equations. (2) and (3). We think that the interfaces are axially symmetric, which means that the magnetization and spin buildup are either parallel to or perpendicular to the interface.

N|N multilayer

We start with a multilayer that has multiple links of metals N1 and N2 that are not magnetic. We'd like to see how the spin current decreases over time. This could include spin relaxation at the edge and in the mass. To do this, we put nodes in both the N1 and N2 layers and look at the case with axially symmetric interfaces that match the relationships Gsc = Gsc = Gm = 0. The conductances Gcc, Gss, Gm 1, and Gm 2 account for the scattering in the mass and/or at the interfaces. Putting Eq. Using (3), we get the spin current equations for each node i in the superlattice.

$$I_i^s = \mathcal{G}^{ss}\left(f_{i-1}^s - f_i^s\right) - \mathcal{G}_i^m f_i^s, \qquad (47)$$

$$I_i^s = \mathcal{G}^{ss}\left(f_i^s - f_{i+1}^s\right) + \mathcal{G}_i^m f_i^s, \qquad (48)$$

This leads to the recursive formula.

$$f_s^i = C_1 e^{\delta i} + C_2 e^{-\delta i}, \qquad (50)$$

where the border conditions set the values of C1 and C2. We get the leading term for the rate of decay in the case of weak spin-flip scattering:

$$\delta^2 \approx \frac{\mathcal{G}_1^m + \mathcal{G}_2^m}{G^{cc}}, \qquad (51)$$

where the border conditions set the values of C1 and C2. Equation only has a negative. this is true for the spin-flip processes with the lowest order. The Sharvin resistance must be used to renormalize (51) for clear Ohmic links. This is done by writing 1/G cc = 1/Gcc (1/M1 + 1/M2)/(4G0). The constant makes it easy to see how the spin current decreases as the superlattice's number of layers grows. Eq. The conductances are shown in 1. (51) may also include bulk scattering, and the total conductances can be found by adding the bulk and surface conductances together using Equations. (2) and (3). When using experimental data to get Eq., only interfacial effects are usually taken into account. (51), but the main efforts are just taken away [1]. This doesn't matter if the spin-orbit contact is small; the overall Gm is just the sum of the contributions from the interface and the bulk.

F|N and F|F multilayers

To measure spin relaxation at magnetic surfaces, look at F|N and F|F multilayers connected to ferromagnetic leads [1]. In this case, the scattering matrix elements and generalized conductances in Eq. can also be linked to a measure that shows how the spin current decreases. (2) and (3). We think about a superlattice that has several points where the nonmagnetic (N1) and ferromagnetically active (F2) layers

International Journal of Integrated Academic Research
ISSN: 3139-5287 | Volume-1 Issue-2 | April-June 2026 | IAR12-005
doi: https://doi.org/10.5281/zenodo.22325761

meet. In this section, nonmagnetic can be thought of as a special case of F. The formulae that follow are the same for F|F multilayers. The loss of spin current due to spin relaxation at the interfaces and in the mass is what we want to look at. We look into nodes in the F and N layers that have connections that are symmetric along the axes. There is also the possibility of collinear spin transport, where the magnetization is in the same plane as the surfaces or goes across them. Generalized conductances can take into account scattering both in the bulk and at the surfaces. Using Math Equations. We get the spin and charge current equations in node i in this way from (2) and (3).

$$I_i^0 = G^{cc}\left(f_{i-1}^0 - f_i^0\right) + G_{i-1}^{cs}\left(f_{i-1}^s - f_i^s\right) - G_i^m f_i^s, \quad (52)$$

$$I_i^0 = G^{cc}\left(f_i^0 - f_{i+1}^0\right) + G_{i+1}^{cs}\left(f_i^s - f_{i+1}^s\right) + G_i^m f_i^s, \quad (53)$$

$$I_i^s = G_{i-1}^{sc}\left(f_{i-1}^0 - f_i^0\right) + \mathcal{G}^{ss}\left(f_{i-1}^s - f_i^s\right) - \mathcal{G}_i^m f_i^s, \quad (54)$$

$$I_i^s = G_{i+1}^{sc}\left(f_i^0 - f_{i+1}^0\right) + \mathcal{G}^{ss}\left(f_i^s - f_{i+1}^s\right) + \mathcal{G}_i^m f_i^s, \quad (55)$$

which leads to the formula that repeats itself:

$$\frac{2\mathcal{G}_i^m/G_{i-1}^{sc} - 2G_i^m/G^{cc}}{\mathcal{G}^{ss}/G_{i-1}^{sc} - G_{i-1}^{cs}/G^{cc}} f_i^s = f_{i-1}^s - 2f_i^s + f_{i+1}^s. \quad (56)$$

Like the case where the material isn't magnetic, the previous problem can be solved analytically:

$$f_s^i = C_1 e^{\delta i} + C_2 e^{-\delta i}. \quad (57)$$

We get the leading term for the rate of decay in the case of weak spin-flip scattering:

$$\delta^2 \approx \frac{\mathcal{G}_F^m + \mathcal{G}_N^m}{G^*}, \quad (58)$$

The effective conductance of the scattering area is given by G = [(Gcc) 2 (Gsc) 2]/Gcc. Equation only has a negative. applies to the spin-flip processes with the lowest order. The Sharvin resistance must be used to renormalize (58) for open Ohmic links. This is done by writing 1/G = 1/G (1/M 1 + 1/M 1 + 1/M 2 + 1/M 2)/(8G0). As the number of levels in the multilayers goes up, the constant shows how the spin current decreases. The conductances shown in Eq. are the same as they were in N|N. (58) might also have mass scattering. Equations can be used to join the conductances at the bulk and contact. (2) and (3).

SPIN-ORBIT TORQUE

The theory of circuits (Eqs. shows a break in the spin current at the contact. You can use (2) and (3) to figure out the total force that is applied to both the magnetization and the lattice. In general, telling these two contributions apart takes more than just circuit theory. Circuit theory can be used to figure out the spin torque on magnetism when exchange interactions are strong and the torque on the lattice can be ignored. It is important to note that spin-flip dispersion and spin memory loss can happen even when there is no lattice torque. This could be because of magnetic disorder at the contact, for example. Since there is no rotational momentum transfer to the lattice, it makes sense to assume axial symmetry in the direction of magnetization. This makes Equations easier to understand. In other words, x(2) 1 = 0, x(0) 1 = x(0) 2, x(1) 1 = x(1) 2 = x(1) 3, x(2) 2 = 0, x(2) 3 = x(2) 4 = x(2) 5 = x(2) 1. And so on. This makes it possible to use Eq. (19) This is how you can find the spin-mixing conductance:

$$\hat{\mathcal{G}}^m = 2\mathcal{G}_r^{\uparrow\downarrow}(\hat{1} - \mathbf{m}\otimes\mathbf{m}) + 2\mathcal{G}_{\parallel}^m \mathbf{m}\otimes\mathbf{m} + 2\mathcal{G}_i^{\uparrow\downarrow}\mathbf{m}\times, \quad (59)$$

It's written as G r = G0 mn Re(nm r mn r mn t mn t mn), which means transverse spin current absorption, and Gm = G0(T + T + R + R), which means longitudinal spin

International Journal of Integrated Academic Research
ISSN: 3139-5287 | Volume-1 Issue-2 | April-June 2026 | IAR12-005
doi: https://doi.org/10.5281/zenodo.22325761

current absorption (also called spin memory loss). G i = G0 mn Im(nm r mn r mn t mn) means spin precession. Even if the formal formulas for G r and G i remained unchanged from Eq. The unitarity of the scattering matrix means that spin-flip scattering can still change their values. On the other hand, there is no straight link between the unitarity restriction and the spin memory loss parameter [29]. Using a normal spin-orbit torque shape and Eq. (3), to find the torque, we can write the following boundary condition:

$$\frac{2e^2}{\hbar}\vec{\tau}_F = e(\hat{1} - \mathbf{m}\otimes\mathbf{m})\mathbf{j}^s = (\hat{1} - \mathbf{m}\otimes\mathbf{m})\hat{\mathcal{G}}^m \cdot \boldsymbol{\mu}^s, \quad (60)$$

where s stands for spin accumulation and F for magnetization force. The diffusion equation can be used to get a better idea of the spin current.

$$\nabla^2\boldsymbol{\mu}^s = \boldsymbol{\mu}^s/l_{sf}^2 \quad (61)$$

$$\mathbf{j}^s = -\frac{\sigma}{2e}\partial_z\boldsymbol{\mu}^s + j^{SH}\hat{y}, \quad (62)$$

The contact is not parallel to the z-axis, and j SH is the spin Hall current. We get the usual antidamping and fieldlike torques:

$$\vec{\tau}_F = (\hbar j^{\mathrm{SH}}/2e)\left[\frac{g_r^{\uparrow\downarrow}\tanh\delta/2}{1+2g_r^{\uparrow\downarrow}\coth\delta}\mathbf{m}\times(\mathbf{m}\times\hat{y}) + \frac{g_i^{\uparrow\downarrow}\tanh\delta/2}{1+2g_i^{\uparrow\downarrow}\coth\delta}\mathbf{m}\times\hat{y}\right], \quad (63)$$

where g r(i) = (ls f /)G r(i) and is the conductivity of the metal that is not magnetic. Spin memory loss should have a direct effect on spin-orbit torque [18,30–32], but these results don't support that idea. As shown by Eq. The two things that cause spin memory loss and spin-orbit force are separate and have nothing to do with each other (59). When spin-orbit interactions are present, the circuit theory can only tell you the total force acting on the lattice and the magnetization. But it looks like the same thing can be said about the fact that there isn't a direct link between torque and spin memory loss.

4. COMPUTATIONAL DETAILS AND INTERFACE GEOMETRY

The transmittances and reflectances (30) and (31) were calculated using the Landauer-Büttiker method, based on the tight-binding linear muffin-tin orbital (LMTO) approach [44]. Addition of spin-orbit coupling (SOC) changed LMTO potential values [44,45]. LDA was employed for correlation and exchange [46]. We studied metal reactions using the face-centered cubic lattice. Epitaxial surfaces with crystallographic orientations (111) or (001) were thought. The average age lattice parameter for the two lead metals was employed, and lattice relaxations were ignored for the contact. In F|N and F|F systems, spin current and magnetization polarizations were considered to be parallel or perpendicular to the contact. Periodic supercells with at least 12 monolayers of each metal maintained charge and spin levels.

A 512 x 512 mesh was utilized for surface Brillouin zone integration in transport calculations for magnetic systems and a 128 x 128 mesh for nonmagnetic systems. We examined how interfacial mixing affected spin memory loss at Pt|Pd and Au|Pd interfaces. Each side of the contact was layered with metal. Mixing increased from 11% to 50%. An A|B interface with 25% intermixing has two random layers of A0.75B0.25 and A0.25B0.75 between the pure A and B leads. The supercell's horizontal size was 2 2 when 25% and

ISSN: 3139-5287 | Volume-1 Issue-2 | April-June 2026 | IAR12-005
doi: https://doi.org/10.5281/zenodo.22325761

50% of the cells mixed, and 3 3 when 11% mingled. Conductances were averaged across all configurations in the 2 2 supercell. Conductances were averaged over 18 random configurations in the 3 3 supercell. We examined a model with long-range intermixing (LRI), where pure A to pure B changes across 8 mixed monolayers (A8/9B1/9, A7/9B2/9,..., A1/9B8/9). This model uses three three-cells.

ADIABATIC EMBEDDING

The scattering zone in the Landauer-Büttiker method is between two perfect semi-infinite leads. Circuit theory holds that the leads are incorporated into the circuit nodes on both sides of the contact. We disable SOC in the leads to create spin-dependent scattering matrices for well-defined spin bases. We recommend "ramp-up" zones between the interface and SOC-free leads to avoid incorrect spreading at interface edges. In these zones, the SOC steadily rises from zero at the active region's boundaries to its true value near the interface. The SOC parameters are scaled by (L 2|x|)/(L 2l0) for an atom x from the interface and |x| > l0. L is the active region length and l0 is the region on each side of the interface where SOC is full strength.

We set l0 to two monolayers for math. A steadily shifting potential allows only minimal momentum transfer for dispersion. This adi abatic embedding [29] evolves a pure spin state from the lead without scattering before scattering at the interface. If the metal is not magnetic, adiabatic embedding causes a lot of reflection at the Fermi surface lines where the group velocity is parallel to the contact (Ref. [29]). These lines form the projected Fermi surface edge when projected orthogonally onto the contact plane. These wave vectors allow electrons to bounce and spin flip from the SOC ramp-up area. Adiabatic embedding causes spin-flip reflectivity backscattering, which must be removed [29]. This backscattering doesn't modify a magnetic lead's spin, so it doesn't affect spin memory loss predictions.

Adiabatic embedding can disperse Fermi surface sheets where they intersect. Because an electron can migrate between sheets with a little momentum change. This study found crossings in all ferromagnetic transition metals but not in nonmagnetic metals Cu, Ag, Au, Pd, and Pt. Scattering from one sheet to another is a spin-flip because the sheets meet with opposite spin states. This scattering may change propagation direction relative to the interface depending on the signs of the normal (to the interface) components v of the group velocities at the crossing. Spin-flip reflection or transmission can occur. Figure 1 depicts these two situations. 1. If v on the two crossing sheets has opposing signs [see Figs. 1(a) and 1(b)], SOC opens a gap at the avoided crossing. A spin flip from the ramp-up region totally reflects electrons that reach the gap with quasimomenta near the intersection. However, if both sides of v have the same sign [Figs. As it goes through the ramp-up zone, the electron may forward spin-flip scatter instead of backscatter. Since we're interested in interface spin-flip dispersion, the role of

International Journal of Integrated Academic Research
ISSN: 3139-5287 | Volume-1 Issue-2 | April-June 2026 | IAR12-005
doi: https://doi.org/10.5281/zenodo.22325761

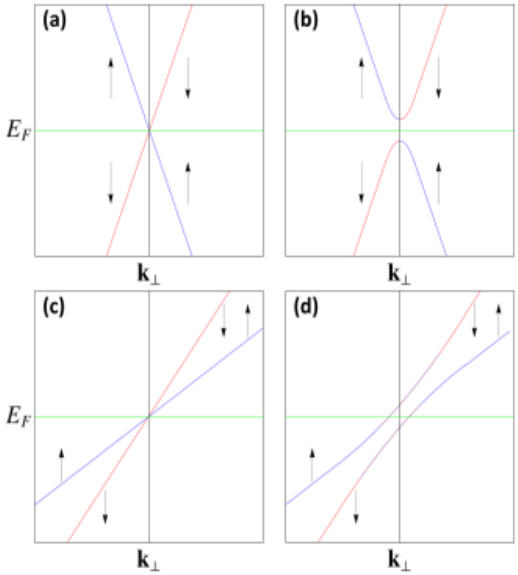


FIG. 1. There is an electronic band crossing in a ferromagnetic lead close to where two Fermi surface sheets with opposite spins meet. This is the stable parallel part of the quasimomentum, denoted by k. (a)–(b) and (c)–(d) show what happens when the normal part of the group velocity v on the two sheets has the same sign or the opposite sign, which leads to resonance spin-flip reflection or transmission. Answers (a) and (c): There is no SOC. (b) and (d): crossovers caused by SOC were prevented.

Due to the ramp-up zones in the leads, spin-flip spreading should be gotten rid of. It's too bad that this can only be done roughly. In Reference [29], the spin-flip reflectances of two extra systems, N1|N1 and N2|N2, were taken away. In these systems, the same lead material is used on both sides of a made-up interface with adiabatic embedding. In the real N1|N2 system, electrons that hit one of the leads and were reflected by the ramp-up region never made it to the interface, so this process makes sense. We can say the same thing about backscattering on Fermi sheet crosses in F in a F|N system [see Figs. 1(a) and 1(b), but not for forward scattering [see Figs. 1(a) and 1(b)]. 1, lines (c) and (d)]. Still, we apply the method from Reference [29] to the F|N interfaces as a rough estimate, leaving out the spin-flip reflectances in auxiliary F|F and N|N systems as well as the spin-flip transmittance in auxiliary F|F. For an F1|F2 link, we also take the difference between the reflectances and transmittances in F1|F1 and F2|F2. This means that for any kind of interface, we define

$$T'_{\uparrow\downarrow} = T^{1|2}_{\uparrow\downarrow} - T^{1|1}_{\uparrow\downarrow} - T^{2|2}_{\uparrow\downarrow}, \tag{64}$$

$$R'_{a,\uparrow\downarrow} = R^{1|2}_{a,\uparrow\downarrow} - R^{a|a}_{\uparrow\downarrow}, \tag{65}$$

where Equation 10 uses primed amounts and an is a line. This procedure is called the "subtraction approach," and the value is "s."

Finding areas in the surface Brillouin zone where unwanted reflection or transmission occurs and removing spin-flip scattering inputs from those spots is a more thorough method. Careful filtering is needed because certain spin-flip scattering events near Fermi surface crossings are produced by physical errors, not adiabatic embedding defects. Figure 1 displays this. 2, which shows how crossing spin Fermi sheets at opposite ends of the spectrum might simplify spin-flip scattering. Left lead spin-flip backscattering is shown in Figure 2(a). In a non-magnetic metal, this can happen near a Fermi projection border or a Fermi crossover like Figure 2. 1(b). Figures show steps. Fig. 2(b) and 2(c) demonstrate Fermi crossing forward scattering. An electron hits lead 1(d) on the left side and either passes or bounces. The reverse of each step works the other way. Three steps are shown in figures.

International Journal of Integrated Academic Research
ISSN: 3139-5287 | Volume-1 Issue-2 | April-June 2026 | IAR12-005
doi: https://doi.org/10.5281/zenodo.22325761

Only a ramp-up area can give the tiny momentum needed for scattering between Fermi sheets, hence 2(a) and 2(c) exist. Compared to Figs. Physical scattering steps are presented in Figures 2(d) and 2(e). This time, the spin-orbit gap in Fig. 1 contains the left lead electron's speed.1(b) leading right. At [2(e)], the electron undergoes resonant spin-flip transmission [Fig. 2(d)] or reflection [Fig.]. Figure 1 shows resonant spin-flip transfer. 2(d) is feasible because an electron can scatter to a different Fermi sheet and gain momentum from touching. Pictures are in Figures 1 and 2. 2(d) and 2(e) are simple because the right lead's spin-orbit gap has little wave function. Let's start with spin-flip scattering in non-contact systems. Only adiabatic embedding produces scattering here. Figures 1 and 2 illustrate spin-flip reflection at Fermi projection edges. In Figure 3(a) and 3(d), adiabatically implanted Pt and Pd form a fake "interface" of a material with itself (Pd|Pd) [29]. Pt has a greater spin orbit constant than Pd. This means strong spin-flip reflection zones are larger. Figures exhibit spin-flip reflections at Fermi crossings. Figs. 4(a) and 4(b) demonstrate adiabatically inserted Ni and Co. These two instances mirror Fig. 2(a). Figs. 1 and 2 illustrate spin-flip transfer at Fermi crossings in Ni and Co. 4(c) and 4(d). 2(b) excludes the physical link. Consider actual linkages. Contours with high spin-flip reflection, like Fig. Figure 3(d) for Pd|Pd is also there. Fig. 3(c) shows electrons from the Pd lead in Pt|Pd. Figs. 4(a) and 4(g) show Ni|Ni and Ni|Co, respectively. Figure 1 depicts these steps. 1(a). The shapes in Fig. 4(c) for Ni|Ni appear in both photographs. For spin-flip trans mission and reflection, Ni|Co 4(e) and 4(g) are presented. The steps are in Figs. 2(c) and 2(b). Resonant forms

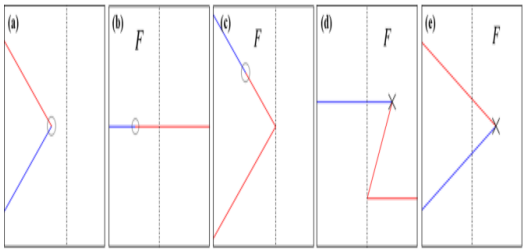


FIG. 2. Spin-flip scattering occurs when two Fermi sheets with opposite spins cross in a smooth, adiabatically embedded surface. Dashed straight lines indicate the contact; F indicates ferromagnetic metal. The blue and red lines illustrate an electron's pre- and post-spin positions. Crosses indicate physical spin-flip dispersion, while circles indicate adiabatic embedding solely.

In the Ni|Co spin-flip transfer [Fig. 4(d)], they also appear. This matches Figure 4(e). 2(b), but the lines flipped. Each spin-flip scattering process in Figs. 2(a)–2(c) is an adiabatic embedding artifact that must be eliminated to determine the interfacial spin loss value. However, spin-flip transmission and reflection [Fig. 4(e)] The Ni|Co contact functions exhibit spin-flip resonances in Figs. 2(e) and 2(d). See the spin-flip reflection function for electrons from the Ni lead at the Ni|Co contact in Fig. 1. 4(g). Figure 2 illustrates other resonant outlines. Spin-flip reflection and transmission in Ni|Ni are shown in Figs. 4(a) and 4(c). 4(g) that fit Fig. 4(b) Co|Co spin-flip reflection resonances. Fig. 4(e) shows Ni|Co spin-flip transfer resonant forms that match Fig. 2(d). Figure 1 shows the same physical process as these resonances. 2(e) shouldn't be ignored while calculating spin-loss. This study demonstrates genuine resonant spin-flip

International Journal of Integrated Academic Research
ISSN: 3139-5287 | Volume-1 Issue-2 | April-June 2026 | IAR12-005
doi: https://doi.org/10.5281/zenodo.22325761

scattering processes and adiabatic embedding artifacts [Figs. 2(a)–2(c)]. 2(a)-2(c)]. Use support system spin-flip transmission functions to find 2(d) and 2(e) in k space. Instead of subtraction, k-point filtering can remove adiabatic embedding effects. Find the k sites on nonmagnetic (N1|N2) interfaces where the spin-flip reflectance in an auxiliary system (N1|N1 or N2|N2) exceeds a threshold. After removing the k points' contributions, the auxiliary system's spin-flip reflectance is less than 0.001G0. Next are contributions from

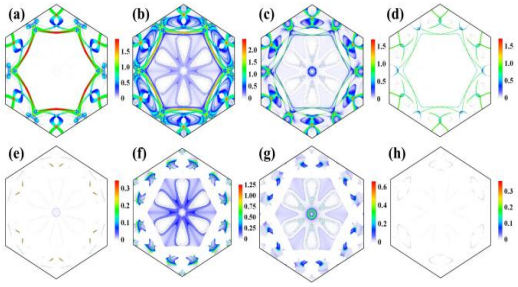


FIG. 3. Spin-flip reflection works with and without k-point filtering for Pt|Pt, Pd|Pd, and Pt|Pd surfaces that are embedded adiabatically. A) R in Pt|Pt; B) RL in Pt|Pd; C) RR in Pt|Pd; D) R in Pd|Pd; E) filtered R in Pt|Pt; F) filtered RL in Pt|Pd; G) filtered RR in Pt|Pd; and H) filtered R in Pd|Pd.

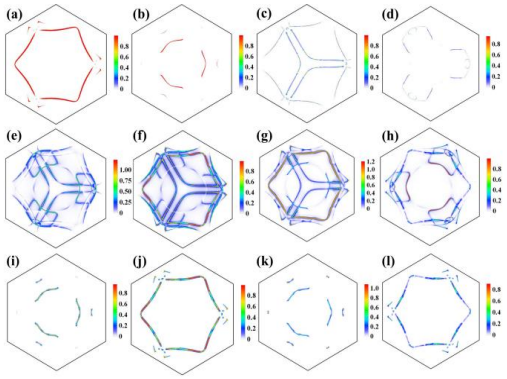


FIG. 4. To show how k-point filtering works, we'll look at spin-flip transmission and reflection functions for Ni|Ni, Co|Co, and Ni|Co. (a) R in Ni|Ni; (b) R in Co|Co; (c) T in Ni|Ni; (d) T in Co|Co; (e) T in Ni|Co; (f) T in Ni|Co; (g) RL in Ni|Co; (h) RR in Ni|Co; (i) filtered T in Ni|Co; (j) filtered T in Ni|Co; (k) filtered RL in Ni|Co;

When figuring out the spin-flip reflectance for electrons sent out from the matched lead, the k points are taken out. To make sure that the objects are gone for good, the omitted zones are slightly stretched out. Ferromagnetic leads cause resonant scattering near where two different spins cross the Fermi surface. Things that happen like the ones in Figs. As was already said, 2(a)–2(c) should be thrown out. We found that resonant processes control the spin-flip reflectances and transmittances for all of the ferromagnetic surfaces we looked at. 2(d) and 2(e), not just general k-point additions. The spin-loss values that were found after taking out the steps shown in Figs. 2(a)–2(c), or by leaving out the ones in Figs. It's almost the same between 2(d) and 2(e). The spin-flip scattering functions from Figures are shown in Figures 4(i)–4(l). 4(e)–4(h) and taking out everything that isn't shown in Figs. 2(e) and 2(d). By using k-point filtering in this way, we get a lower bound on the spin flip scattering functions and the spin-loss parameter. This makes sure that the effects of adiabatic embedding are completely removed. This is how the f numbers in Table III were found.

5. RESULTS

It shows the area-resistance products AR and the spin loss values for contacts that are not magnetic in Table I. The subtraction and k-point filtering approaches give comparable values of. For all material combinations, is relatively similar for (001) and (111) interfaces,

International Journal of Integrated Academic Research
ISSN: 3139-5287 | Volume-1 Issue-2 | April-June 2026 | IAR12-005
doi: https://doi.org/10.5281/zenodo.22325761

suggesting that the interface's crystallographic structure has no effect on interfacial spin relaxation. The spin-loss parameter is slightly smaller in all situations when the spin accumulation is parallel to the interface. The computed AR products and parameters agree well with experimental observations [1] in systems lacking Pd, but both are significantly overstated at (Au,Ag,Cu,Pd)|Pd interfaces. However, the results for the Au|Pd (111) interface with spin buildup parallel to the interface match well with Gupta et al. [47] (AR = 0.81 f).

Based on a study of the local spin currents near the interface, m2 and = 0.43) were calculated. The huge disparity in AR for interfaces with Pd suggests that the idealized interface model is insufficient for the situation.

TABLE I. AR (fm2) and spin-loss parameters found for nonmagnetic contacts using the subtraction approach (s) and the filtering method (f). M defines the spin accumulation's orientation relative to the interface.

N|N	Plane	M	AR	AR_{sp}	δ_s	δ_f	δ_{sp}
Pt|Pd	001	∥	0.42	0.14 ± 0.03	0.60	0.57	0.13 ± 0.08
	001	⊥	0.44	0.14 ± 0.03	0.71	0.65	0.13 ± 0.08
	111	∥	0.28	0.14 ± 0.03	0.41	0.36	0.13 ± 0.08
	111	⊥	0.29	0.14 ± 0.03	0.45	0.38	0.13 ± 0.08
Au|Pd	001	∥	0.96	0.23 ± 0.08	0.71	0.68	0.08 ± 0.08
	001	⊥	0.96	0.23 ± 0.08	0.86	0.82	0.08 ± 0.08
	111	∥	0.83	0.23 ± 0.08	0.53	0.54	0.08 ± 0.08
	111	⊥	0.87	0.23 ± 0.08	0.73	0.69	0.08 ± 0.08
Ag|Pd	001	∥	0.92	0.35 ± 0.08	0.41	0.47	0.15 ± 0.08
	001	⊥	1.12	0.35 ± 0.08	0.50	0.54	0.15 ± 0.08
	111	∥	0.89	0.35 ± 0.08	0.41	0.47	0.15 ± 0.08
	111	⊥	0.92	0.35 ± 0.08	0.50	0.55	0.15 ± 0.08
Cu|Pd	001	∥	0.81	0.45 ± 0.005	0.41	0.47	0.24 ± 0.05
	001	⊥	0.81	0.45 ± 0.005	0.47	0.52	0.24 ± 0.05
	111	∥	0.80	0.45 ± 0.005	0.43	0.40	0.24 ± 0.05
	111	⊥	0.81	0.45 ± 0.005	0.53	0.48	0.24 ± 0.05
Cu|Au	001	∥	0.13	0.15 ± 0.005	0.08	0.08	0.13 ± 0.07
	001	⊥	0.13	0.15 ± 0.005	0.11	0.11	0.13 ± 0.07
	111	∥	0.11	0.15 ± 0.005	0.08	0.07	0.13 ± 0.07
	111	⊥	0.12	0.15 ± 0.005	0.11	0.10	0.13 ± 0.07
Cu|Pt	001	∥	0.90	0.75 ± 0.05	1.00	0.87	0.9 ± 0.1
	001	⊥	0.89	0.75 ± 0.05	1.07	0.9	0.9 ± 0.1
	111	∥	0.75	0.75 ± 0.05	0.88	0.72	0.9 ± 0.1
	111	⊥	0.82	0.75 ± 0.05	1.11	0.83	0.9 ± 0.1
Cu|Ag	001	∥	0.03	0.045 ± 0.005	0.02	0.2	0
	001	⊥	0.03	0.045 ± 0.005	0.03	0.02	0
	111	∥	0.13	0.045 ± 0.005	0.03	0.03	0
	111	⊥	0.13	0.045 ± 0.005	0.04	0.04	0

interfaces. As a result, Pt|Pd and Au|Pd with interfacial intermixing were also built, as described in Sec. Table II shows the results for intermixed interfaces; it is clear that intermixing raises the AR product, whilst its values for ideal interfaces with Pd are already excessively large when compared to experimental reports. Intermixing also greatly increases the spin-loss parameter, pushing it further away from experimental data.

TABLE II. Table I relates to nonmagnetic contacts with intermixing. The percentage reflects the content of the two intermixed layers. LRI is an abbreviation for the long-range intermixing model (see Sec. V for more information

N|N (mix %)	Plane	M	AR	AR_{sp}	δ_s	δ_f	δ_{sp}
Pt|Pd (11%)	111	∥	0.29	0.14 ± 0.03	0.45	0.38	0.13 ± 0.08
	111	⊥	0.30	0.14 ± 0.03	0.56	0.40	0.13 ± 0.08
Pt|Pd (25%)	111	∥	0.32	0.14 ± 0.03	0.52	0.46	0.13 ± 0.08
	111	⊥	0.34	0.14 ± 0.03	0.65	0.52	0.13 ± 0.08
Pt|Pd (50%)	111	∥	0.36	0.14 ± 0.03	0.58	0.51	0.13 ± 0.08
	111	⊥	0.38	0.14 ± 0.03	0.72	0.57	0.13 ± 0.08
Pt|Pd (LRI)	111	∥	0.82	0.14 ± 0.03	1.20	0.91	0.13 ± 0.08
	111	⊥	0.85	0.14 ± 0.03	1.34	0.96	0.13 ± 0.08
Au|Pd (11%)	111	∥	0.86	0.23 ± 0.08	0.56	0.46	0.08 ± 0.08
	111	⊥	0.90	0.23 ± 0.08	0.76	0.58	0.08 ± 0.08
Au|Pd (25%)	111	∥	0.96	0.23 ± 0.08	0.60	0.58	0.08 ± 0.08
	111	⊥	1.01	0.23 ± 0.08	0.81	0.73	0.08 ± 0.08
Au|Pd (50%)	111	∥	0.95	0.23 ± 0.08	0.60	0.58	0.08 ± 0.08
	111	⊥	0.99	0.23 ± 0.08	0.82	0.73	0.08 ± 0.08
Au|Pd (LRI)	111	∥	1.24	0.23 ± 0.08	0.79	0.65	0.08 ± 0.08
	111	⊥	1.29	0.23 ± 0.08	0.98	0.76	0.08 ± 0.08

TABLE III. The same as in Table I, except for the F|N and F|F connections.

F(N)|F	Plane	M	AR_1	AR_2	AR	AR_{sp}	δ_s	δ_f	δ_{sp}
Cu|Co	001	∥	0.29	2.06	0.59	0.51 ± 0.05	0.22	0.12	0.33 ± 0.05
	001	⊥	0.31	2.05	0.59	0.51 ± 0.05	0.24	0.14	0.33 ± 0.05
	111	∥	0.36	1.54	0.48	0.51 ± 0.05	0.18	0.11	0.33 ± 0.05
	111	⊥	0.36	1.52	0.47	0.51 ± 0.05	0.19	0.12	0.33 ± 0.05
Pt|Co	001	∥	0.46	4.67	1.28	0.85 ± 0.12	1.12	0.91	0.9 ± 0.4
	001	⊥	0.44	4.60	1.26	0.85 ± 0.12	1.17	0.96	0.9 ± 0.4
	111	∥	1.70	1.36	0.76	0.85 ± 0.12	0.81	0.72	0.9 ± 0.4
	111	⊥	1.82	1.38	0.80	0.85 ± 0.12	0.91	0.80	0.9 ± 0.4
Ag|Co	001	∥	0.40	1.87	0.57	0.56 ± 0.06	0.33	0.21	0.33 ± 0.1
	001	⊥	0.43	1.84	0.57	0.56 ± 0.06	0.38	0.29	0.33 ± 0.1
	111	∥	0.22	1.58	0.45	0.56 ± 0.06	0.20	0.12	0.33 ± 0.1
	111	⊥	0.22	1.57	0.45	0.56 ± 0.06	0.21	0.13	0.33 ± 0.1
Ni|Co	001	∥	0.22	1.04	0.32	0.255 ± 0.025	0.32	0.15	0.35 ± 0.05
	001	⊥	0.24	1.02	0.32	0.255 ± 0.025	0.34	0.16	0.35 ± 0.05
	111	∥	0.21	0.73	0.23	0.255 ± 0.025	0.27	0.17	0.35 ± 0.05
	111	⊥	0.25	0.72	0.24	0.255 ± 0.025	0.29	0.16	0.35 ± 0.05

The disparity in the values of AR and for interfaces with Pd with experiment is most likely owing to a lack of understanding of the interfacial structure in the sputtered

ISSN: 3139-5287 | Volume-1 Issue-2 | April-June 2026 | IAR12-005
doi: https://doi.org/10.5281/zenodo.22325761

mul tilayers, for which no structural characterisation is available to our knowledge. It appears doubtful that real sputtering interfaces are considerably less resistive than ideal or intermixed interfaces considered here. It is probable that nominally bulk portions in sputtered multilayers containing Pd are more disordered than pure Pd films, resulting in greater resistivity and shorter spin-diffusion length. The fitting approach used to obtain the AR and interface parameters [1] would then attribute this additional bulk resistance and spin relaxation to the interfaces. B. Table III shows the results for ferromagnetic interfaces with one or two ferromagnetic leads. The AR products for all interfaces agree perfectly with the experimental data [1]. When compared to the k-point filtering approach (f), the values of the spin-loss parameter produced using the subtraction method (s) tend to be bigger by up to a factor of two. The results for AR and for Pt|Co are in good agreement with observation and computations using the discontinuity of the spin current. [47] In some systems, AR corresponds extremely well with experiment but is overestimated, which could be related to a failure to account for interfacial disorder and the constraints of the adiabatic-embedding method.

6. CONCLUSIONS

A broad method for studying magnetoelectronic circuits with spin-nonconserving N|N, F|N, or F|F interfaces between diffusive bulk areas has been created. All potential spin-nonconserving processes, such as spin dephasing, spin loss, and spin precession, are represented by a tensor generalization of the spin-mixing conductance. When exchange interactions rule, those contributions can be clearly split into components that are responsible for spin memory loss, spin-orbit torque, and spin precession. Surprisingly, no direct relationship exists between spin-orbit torque and spin memory loss; the two effects are characterized by different combinations of scattering amplitudes that are responsible for the absorption of the transverse and longitudinal components of spin current at the interface.

The spin relaxation (i.e., spin memory loss) parameter has been found numerically using Eqs. (51) and (58), respectively, for a range of N|N, F|N, and F|F interfaces. With the exception of N|N interfaces containing a Pd lead, first-principles calculations using adiabatic embedding show reasonable agreement with experiment for and the area-resistance products. Both and AR are greatly overstated for such surfaces, which cannot be explained by short- or long-range interfacial intermixing. The analysis of spin-flip scattering probabilities for F|N and F|F interfaces shows that electronic states near the crossings of the Fermi surfaces for opposite spins in ferromagnets dominate interfacial spin relaxation. The extended magnetoelectronic circuit theory provides a useful framework for studying spin transport in magnetic nanostructures with significant spin-orbit interaction at interfaces.

REFERENCE

1. J. Bass, J. Magn. Magn. Mater. 408, 244 (2016).
2. J. Bass and W. P. Pratt, Jr., J. Phys.: Condens. Matter 19, 183201 (2007).

ISSN: 3139-5287 | Volume-1 Issue-2 | April-June 2026 | IAR12-005
doi: https://doi.org/10.5281/zenodo.22325761

3. M. Johnson and R. H. Silsbee, Phys. Rev. Lett. 55, 1790 (1985).
4. D. Ralph and M. Stiles, J. Magn. Magn. Mater. 320, 1190 (2008).
5. O. Mosendz, J. E. Pearson, F. Y. Fradin, G. E. W. Bauer, S. D. Bader, and A. Hoffmann, Phys. Rev. Lett. 104, 046601 (2010).
6. B. Heinrich, C. Burrowes, E. Montoya, B. Kardasz, E. Girt, Y.-Y. Song, Y. Sun, and M. Wu, Phys. Rev. Lett. 107, 066604 (2011).
7. Y. Tserkovnyak, A. Brataas, G. E. W. Bauer, and B. I. Halperin, Rev. Mod. Phys. 77, 1375 (2005).
8. L. Liu, C.-F. Pai, Y. Li, H. W. Tseng, D. C. Ralph, and R. A. Buhrman, Science 336, 555 (2012).
9. V. E. Demidov, S. Urazhdin, H. Ulrichs, V. Tiberkevich, A. Slavin, D. Baither, G. Schmitz, and S. O. Demokritov, Nat. Mater. 11, 1028 (2012).
10. Y.-T. Chen, S. Takahashi, H. Nakayama, M. Althammer, S. T. B. Goennenwein, E. Saitoh, and G. E. W. Bauer, Phys. Rev. B 87, 144411 (2013).
11. G. E. W. Bauer, E. Saitoh, and B. J. van Wees, Nat. Mater. 11, 391 (2012).
12. H. Adachi, K.-I. Uchida, E. Saitoh, and S. Maekawa, Rep. Prog. Phys. 76, 036501 (2013).
13. D. Meier, D. Reinhardt, M. van Straaten, C. Klewe, M. Althammer, M. Schreier, S. T. B. Goennenwein, A. Gupta, M. Schmid, C. H. Back et al., Nat. Commun. 6, 8211 (2015).